Calcium-selective electrodes based on photo-cured polyurethane-acrylate membranes covalently attached to methacrylate functionalized poly(3,4-ethylenedioxythiophene) as solid-contact

Ocana Tejada, Cristina; Abramova, Natalia; Bratov, Andrey; Lindfors, Tom; Bobacka, Johan

Published in:
Talanta

DOI:
10.1016/j.talanta.2018.04.056

Published: 01/01/2018

Document Version
Accepted author manuscript

Document License
CC BY-NC-ND

Calcium-selective electrodes based on photo-cured polyurethane-acrylate membranes covalently attached to methacrylate functionalized poly(3,4-ethylenedioxythiophene) as solid-contact

Cristina Ocaña[1,2] , Natalia Abramova[1,3], Andrey Bratov*[1], Tom Lindfors[2] and Johan Bobacka*[2]

[1] BioMEMs Group, Instituto de Microelectrónica de Barcelona, Centro Nacional de Microelectrónica (IMB-CNM-CSIC), Campus UAB, Bellaterra, 08193, Spain.

[2] Laboratory of Analytical Chemistry, Faculty of Science and Engineering, Johan Gadolin Process Chemistry Centre, Åbo Akademi University, Biskopsgatan 8, FIN-20500, Turku-Åbo, Finland.

[3] Laboratory of Artificial Sensors Systems, ITMO University, Kronverskiy pr. 49, St. Petersburg 197101, Russia.

*Corresponding author: email: andrei.bratov@imb-cnm.csic.es / jbobacka@abo.fi

Abstract

We report here the fabrication of solid-contact calcium-selective electrodes (Ca^{2+}-SCISEs) made of a polyurethane acrylate ion-selective membrane (ISM) that was covalently attached to the underlying ion-to-electron transducer (solid-contact). Methacrylate-functionalized poly(3,4-ethylenedioxythiophene) (Meth-PEDOT) and Meth-PEDOT films containing either multiwalled carbon nanotubes (MWCNT) or carboxylated MWCNT (cMWCNT) were used as solid contacts. The solid contacts were deposited by drop-casting on screen-printed electrodes and characterized by cyclic voltammetry (CV), electrochemical impedance spectroscopy (EIS) and potentiometry. Covalent binding between the solid contact and the ISM was obtained via photopolymerization in order to increase the robustness of the Ca^{2+}-SCISEs. The performance of the Ca^{2+}-SCISEs was studied by measuring their potentiometric response and their sensitivity to light, oxygen and carbon dioxide. Meth-PEDOT was found to be a promising solid-contact material to develop low-cost and easy to prepare ISEs.

Keywords: tetramethacrylate poly(3,4-ethylenedioxythiophene), MWCNT, all-solid-state ion-selective electrode, calcium, polyurethane membrane.

1. Introduction

Over the years, the synthesis and characterization of conducting polymers has attracted attention due to their unique electronic and optical properties [1, 2] in many applications such as electrochromic devices [3-5], light emitting diodes [6-8], energy storage devices [9-11], biosensors [12-14] and all-solid-state ion sensors [15-18]. Among electronically conducting polymers, there is a considerable interest in using poly(3,4-ethylenedioxythiophene) (PEDOT) because of its low oxidation potential, high stability in ambient environments [19, 20], mechanical flexibility and stable oxidized form [21]. Furthermore, addition of electrically conducting nanomaterials (e.g. graphene or carbon nanotubes) to PEDOT is known to improve the electrical conductivity by better connecting individual conducting PEDOT domains in the composite film [22, 23].

In this work, methacrylate-functionalized PEDOT (Meth-PEDOT), Meth-PEDOT containing MWCNT (Meth-PEDOT-MWCNT) and cMWCNT (Meth-PEDOT-cMWCNT) were used as the ion-to-electron transducer in potentiometric solid-contact calcium-selective electrodes (Ca^{2+}-SCISEs). In recent years, the classical liquid contact ISEs are being replaced by SCISEs due to the possibility of robust miniaturization [24], low-cost production and compatibility with mass production by standard microfabrication techniques [25]. Most of the reported SCISEs with conductive polymers use plasticized poly(vinyl chloride) (PVC) as the ion-selective membrane (ISM) [26-28]. However, the PVC-based ISEs suffer from diffusion of water through the ISM and the possible formation of a water layer or water pools at the ISM/solid-contact (SC) or SC/substrate interfaces resulting in poor potential stability and weakening of the ISM adhesion to the substrate [29, 30].

Photocurable membranes are alternative materials to PVC-ISMs. Several ISEs using photocurable ISMs have been developed since their introduction in the middle of 1980s and 1990s [31, 32]. Photo-cured polymeric systems show many advantages over PVC-ISMs such as the possibility to use standard photolithography processes,

which may be beneficial for mass production of ISEs, and the opportunity to obtain ISMs with low leaching rates of the active components [33]. Urethane-acrylate ISMs are one of the most used photo-cured membrane types because of their fast curing rates and their compatibility with common plasticizers and ionophores [34]. In addition, this type of ISMs present high durability and reduced biofouling when SCISEs are used in biological samples [35] and they may possibly be chemically "anchored" to the solid electrode substrate [32]. However, it must be noted that it is not the first time that Meth-PEDOT and ISM matrix are copolymerized. Rzewuska et al. reported SCISEs based on the copolymerization of polyacrylate-based membrane and Meth-PEDOT on a glassy carbon electrode surface forming a single phase membrane matrix [36]. However, in this approach the polymerization time was 5 minutes and in our previous studies we observed that when the polymerization time increases the selectivity of the SCISEs becomes worse due to the sodium tetrakis[3,5-bis-(trifluoromethyl)phenyl]borate photobleaching [37].

The main aim of this work is electrochemical characterization of Meth-PEDOT, Meth-PEDOT-MWCNT and Meth-PEDOT-cMWCNT and their application as ion-to-electron transducers in polyurethane (PU) based Ca^{2+}-SCISEs. In this paper, we present a simple, low-cost and robust method for preparing Ca^{2+}-SCISEs, which might be beneficial for different fields such as ranching where they require easy to use and semiautomatic analytical systems with very low costs per analysis. The end-capped methacrylate groups of Meth-PEDOT functioned as reactive sites for obtaining better bonding and stronger adhesion to the PU-acrylate ISM during the copolymerization process. This was expected to enhance the durability of the Ca^{2+}-SCISEs.

2. Experimental

2.1. Chemicals

Tetramethacrylate end-capped poly(3,4-ethylenedioxythiophene) solution (Meth-PEDOT, 0.5 wt% dispersion in propylene carbonate carbonate and p-toluenesulfonate as charge compensating ion), KCl, KNO_3, $CaCl_2$, $Ca(NO_3)_2$ and carboxylated MWCNTs were obtained from Sigma Aldrich. MWCNTs were obtained from DropSens (Oviedo, Spain). Calcium Ionophore II (ETH 129), bis(2-ethylhexyl) sebacate (DOS), potassium tetrakis(p-chlorophenyl)borate (KTpClPB), ETH500 and

hexafluorobutyl acrylate (HFBuA) were obtained from Fluka. Aliphatic urethane diacrylate (oligomer Ebecryl 270), cross-linker and hexanediol diacrylate (HDDA) were from UCB Chemicals and the photoinitiator 2,2- dimethoxy-2-phenylacetophenone (IRG 651) from Ciba-Geigy. All other chemicals used were analytical reagent grade and all solutions were prepared using ultrapure deionized water with the resistivity of 18.2 MΩ cm (Milli-Q system, Millipore, Billerica, MA). Screen-printed electrodes (SPEs) with silver ink and flash gold (d=2 mm) prepared on PET polymer substrates were supplied by FAE (FAE S.A., Spain).

2.2. Meth-PEDOT, Meth-PEDOT-MWCNT/cMWCNT deposition

5.0 µL (2×2.5 µL) of Meth-PEDOT solution containing either 0.2-0.5 wt% MWCNT or cMWCNT solution was drop-cast on the screen-printed electrodes to form SC layers of Meth-PEDOT-MWCNT and Meth-PEDOT-cMWCNT. After that, the electrodes were placed on a heating plate at 50 ºC to increase the evaporation rate of the propylene carbonate solvent. All further experiments were performed at room temperature.

2.3. Ca^{2+}-selective ISM deposition

The photocurable ISM composition was prepared as presented previously [38]. Briefly, the main polymer composition was prepared by mixing the aliphatic urethane diacrylate oligomer Ebecryl 270 with the reactive diluent HDDA and the photoinitiator Irgacure 651 in the ratio (w/w) of 81:17:2. In the next step, 0.3 g of the main polymer composition was dissolved in 0.2 ml THF and the plasticizers DOS and HFBuA, Ca^{2+}-ionophore II and lipophilic salts were then added to this solution. This ISM solution was placed in an ultrasonic bath until it was homogeneous and then left unstirred for several hours to allow evaporation of THF from the solution. This resulted in the following ISM composition: main polymer mixture (56.5 wt%), DOS (20.0 wt%), HFBuA (20.0 wt%), Ca^{2+}-ionophore II (1.0%), KTpClPB (0.5 wt%) and ETH 500 (2.0 wt%).

ISMs were deposited on the screen-printed electrode substrates (Ag and Au) by applying the ISM solution with a microsyringe on the Meth-PEDOT, Meth-PEDOT-MWCNT and Meth-PEDOT-cMWCNT solid-contact layers. After the ISM

deposition, the electrodes were exposed to 365 nm UV light for 20 s using a UV Curing Light Lamp 8141 (Düren, Germany) to form covalent bonds between the ISMs and the acrylate groups of SCs. A scheme of the copolymerization process is shown in Fig.S1. Crosslinking between the PU-ISM and polyaniline functionalized with methacrylate groups was confirmed by FTIR-ATR analysis in previous studies [32]. Therefore, we assume that crosslinking occurs also between the PU-ISM and the Meth-PEDOT used in this work. The thicknesses of the ISM was ca. 200 µm, as measured with a micrometer screw gauge (resolution: 1 µm) after the polymerization process.

2.4. Cyclic voltammetry (CV) and electrochemical impedance spectroscopy (EIS)

Cyclic voltammograms and impedance spectra were recorded by using a one-compartment three-electrode cell connected to the Autolab potentiostat equipped with a frequency response analyzer (AUT20.FRA2-AUTOLAB, Eco Chemie, B.V., The Netherlands). The screen-printed electrodes, a glassy carbon rod and a double junction Ag/AgCl/3 M KCl//0.1 M LiOAc served as the working (WE), auxiliary (AE) and reference electrode (RE), respectively. CVs were recorded between -0.5 V and +0.4 V in 0.1 M KNO_3 at a scan rate $\nu = 0.01$ Vs^{-1}. The impedance spectra were measured at the open circuit potential (E_{dc}) in 0.1 M KNO_3 within the frequency range (f = 10 kHz – 0.01 Hz) using an excitation signal amplitude $\Delta E_{ac} = 10$ mV. The impedance spectra were fitted to equivalent circuits with the ZView software (Scribner Associates Inc., USA).

2.5. Chronopotentiometric measurements

Constant-current chronopotentiograms were recorded in 0.1 M $CaCl_2$ with the Autolab potentiostat described above by passing a constant current of ±1 nA through the Ca^{2+}-SCISEs for 60 s [39].

2.6. Potentiometric measurements

The potentiometric response of the Ca^{2+}-SCISEs was measured in a Faraday's cage with a 16-channel potentiometer (Lawson Labs, Inc., input impedance: 10^{15} Ω) and by using the double junction Ag/AgCl/3M KCl//0.1 M LiOAc as the RE. The Ca^{2+}-SCISEs were preconditioned under stirring in 10^{-3} M $CaCl_2$ for 3 days prior to the

potentiometric measurements. Calibration plots were obtained in $CaCl_2$ solutions from 10^{-7} M to 10^{-2} M by stirring the solutions for 2 min at each concentration. The activity coefficients were calculated according to the Debye-Hückel equation.

The selectivity coefficients towards Na^+, K^+, Mg^{2+}, NH_4^+ and Li^+ ions were determined at 0.1 M concentrations of interfering ions with the mixed solution method recommended by IUPAC [40]. The potentiometric aqueous layer tests were performed by recording the Ca^{2+}-SCISE potentials in 0.1 M $CaCl_2$, 0.1 M NaCl and 0.1 M $CaCl_2$ solutions (in this order). The CO_2 and O_2 sensitivities of the Ca^{2+}-SCISEs were obtained by measuring the potential of the Ca^{2+}-SCISEs in a 0.1 M $CaCl_2$ solution that was purged with pure O_2, N_2 and CO_2 gas in the following sequence: N_2 (1h), O_2 (1h), N_2 (1h), CO_2 (1h), N_2 (1h). The light sensitivity was measured in 0.1 M $CaCl_2$ solution by monitoring the Ca^{2+}-SCISE potentials as the illumination of the electrode surfaces changed in the following order: darkness (30 min), ambient room light (30 min), cold light (30 min), ambient room light (30 min) and darkness (30 min). The Leica CLS 150 XE cold light source (150 W, 21 V) was directed through the electrolyte solution towards the Ca^{2+}-SCISEs surfaces.

3. Results and discussion

3.1. CV and EIS characterizations

According to Nikolskii and Materova, the SCISEs must have reversible transition from ionic to electronic conductivity at the ISM/SC interface and sufficiently high exchange currents in comparison with the current generated by the potential measurement circuitry to obtain a stable electrode potential [40]. These requirements imply that the solid-contact should have a high redox capacitance to become less polarizable and provide a more stable potential [41].

As shown in Fig. 1, the CVs of the Meth-PEDOT, Meth-PEDOT-MWCNT and Meth-PEDOT-cMWCNT films measured after 100 potential cycles in 0.1 M KNO_3 showed the typical oxidation and reduction behavior of PEDOT [42]. The rather symmetrical shape of the CVs of all Meth-PEDOT films indicates high reversibility of the doping process. The Meth-PEDOT-MWCNT/cMWCNT films (containing CNTs) give in general higher oxidation and reduction currents than the Meth-PEDOT film prepared without CNTs. The highest currents are obtained with the Meth-PEDOT film

containing 0.5 wt% cMWCNT. The improved redox behavior is due to the MWCNT and cMWCNT facilitating the formation of a more extended electrically conductive network in the Meth-PEDOT matrix by connecting isolated conducting PEDOT domains, which enhances the electron transfer at the PEDOT-SC/screen-printed electrode interface [43]. The improved redox behavior is more significant for cMWCNT than for MWCNT due to the presence of carboxyl groups, which can more efficiently participate in the charge compensation process of the Meth-PEDOT films during its oxidation and reduction in 0.1 M KNO_3.

The impedance spectra of the Meth-PEDOT and Meth-PEDOT-MWCNT/cMWCNT solid-contacts in Fig. 2a support the results obtained by CV. The impedance spectra show an almost vertical capacitive behavior at low frequencies except for Meth-PEDOT, which shows a typical diffusional behavior indicating slower ion and electron transport than in the other SCs. The impedance data for Meth-PEDOT-MWCNT/cMWCNT was fitted to the equivalent circuit presented in Fig. 2b composed by the solution resistance (R), the finite-length Warburg diffusion element (Z_D) and the constant phase element (CPE) in series. The equivalent circuit is similar to the one developed earlier for electropolymerized PEDOT [40]. The Z_D element is related to the diffusional time constant (τ_D), the pseudocapacitance (C_D) and the diffusion resistance ($R_D = \tau_D / C_D$) [44]. Fig. S2 compare the experimental and fitted EIS data in the form of Nyquist plots and Table S1 summarizes the results of the fittings. The impedance spectrum for Meth-PEDOT (0 wt% MWCNT/cMWCNT) differs from the rest of the electrodes (Fig. 2a) and did not give a good fit to the equivalent circuit in Fig. 2b, as shown in Fig. S2. Therefore, Meth-PEDOT (0 wt% MWCNT/cMWCNT) was left out from the comparison shown in Table S1. As expected, the addition of MWCNTs/cMWCNTs increases the capacitance of Meth-PEDOT (Table S1) since the CNTs interconnect isolated PEDOT segments, thus improving the oxidation and reduction of PEDOT and lowering its resistance. Additionally, charging of the MWCNT/cMWCNT surface may also contribute to the higher capacitance. The CPE and *n* values of 1.10-3.40 mF and 0.94-0.98, respectively, describe almost an ideal capacitor (*n*=1) and the Meth-PEDOT-cMWCNT films show the highest capacitance of all SCs studied here. This assumption is supported by the results of the EIS fittings shown in Table 1 revealing that the Meth-PEDOT-cMWCNTs have the largest redox capacitance (C_D) and the

smallest diffusion resistance (R_D). These data suggest that the Meth-PEDOT-cMWCNT composite films are best suited as solid-contacts among the Meth-PEDOT films studied here for the PU based Ca^{2+}-SCISEs.

3.2. Potentiometric response of the Meth-PEDOT-based solid-contacts

Initially the potentiometric response of the Meth-PEDOT and Meth-PEDOT-MWCNT/cMWCNT films was studied in the absence of calcium ions in KNO_3 solutions with results presented in Fig. 3. The Meth-PEDOT and the Meth-PEDOT-MWCNTs films showed an anionic response at concentrations > 10^{-5} M implying that the small and mobile NO_3^- (in comparison to the bulky immobilized MWCNTs) function as the main charge compensating anion in the oxidation and reduction reaction of Meth-PEDOT according to equations (1) and (2), which includes also electron transfer between Meth-PEDOT and the electronically conducting substrate (electrical contact). We assume that the less bulky *p*-toluenesulfonate (pTS) used originally as the charge compensating anion in the commercial Meth-PEDOT formulation (according to Sigma-Aldrich) is exchanged to NO_3^- in the PEDOT matrix during the conditioning of the electrodes in 0.1 M KNO_3. In Equation (2), we assume (for simplicity) that the MWCNTs have a surface charge close to zero:

$$\text{Meth-PEDOT}^0 + NO_3^- \,/\, pTS^- \rightleftharpoons \text{Meth-PEDOT}^+ NO_3^- + e^- \quad (1)$$

$$\text{Meth-PEDOT}^0 \text{ MWCNT} + NO_3^- \rightleftharpoons \text{Meth-PEDOT}^+ \text{MWCNT } NO_3^- + e^- \quad (2)$$

On the other hand, the potentiometric response of the Meth-PEDOT-cMWCNT films was only slightly anionic indicating that the films exchange both anions and cations, in addition to electron transfer, resulting in a thermodynamically more well-defined ISM/SC interface. The cationic response in presence of mobile Ca^{2+} cations is illustrated by Equation 3:

$$(\text{Meth-PEDOT}^0 \text{ cMWCNT}^-)_2 \, Ca^{2+} \rightleftharpoons (\text{Meth-PEDOT}^+ \text{ cMWCNT}^-)_2 + Ca^{2+} + 2e^- \quad (3)$$

We may also note here that PEDOT electropolymerized in the presence of the immobile and negatively charged polystyrenesulfonate anion (PSS^-) gives a cationic

potentiometric response [19] due to the oxidation-reduction reaction similar to presented in Equation 3.

3.3. Chronopotentiometric measurements with Ca^{2+}-SCISEs

Constant-current chronopotentiometric measurements were performed in order to critically evaluate the potential stability of the different types of Ca^{2+}-SCISEs [19]. The slope ($\Delta E/\Delta t$) of the response curves provides a direct measure of the potential stability of the Ca^{2+}-SCISEs upon passage of a small current. As can be seen in Fig. 4 and Table 1, all Ca^{2+}-SCISEs prepared with the Meth-PEDOT and Meth-PEDOT-MWCNT/cMWCNT solid-contacts showed rather similar potential drifts. From these measurements in Fig. 4, we can estimate the total resistance of the PU-ISM and the SC, and the redox capacitance (C_L) of the SC covered by the PU-ISM. We should point out here that the resistance of the SC is usually negligible compared to that of the ISM. For the Ca^{2+}-SCISEs studied, the bulk resistance is obtained from the potential difference (ΔE) in the chronopotentiograms when the current direction is reversed at t=60s. As expected, all PU-ISMs had relatively high bulk resistances of 86-117 MΩ (Table 1). However, the buried SCs had rather similar redox capacitances varying between 29-47 µF. Especially the Meth-PEDOT and Meth-PEDOT-cMWCNTs had almost identical redox capacitances of 29-35 µF showing that the cMWNCTs do not improve the redox capacitance of the PEDOT-SC in Ca^{2+}-SCISEs. We determined therefore also the redox capacitance of the non-coated Meth-PEDOT and Meth-PEDOT-MWCNT/cMWCNT solid-contacts (without ISM) from the CV and EIS measurements. Table 1 reveals that after deposition of the PU-ISM the capacitances decreased to 3.6-10.7% from their initial values for the uncoated SCs. For the Meth-PEDOT prepared 0.5 wt% cMWCNTs, the redox capacitance dropped to only ca. 1% due to its considerably higher initial capacitance than for the other SCs. It can thus be concluded that the redox process of the SCs beneath the ISM and the ion transport associated with it, which is necessary for the oxidation and reduction reaction of Meth-PEDOT, is hampered by the PU-ISM [39].

3.4. Calibration of the Ca^{2+}-SCISEs

Fig. 5a shows the potentiometric response of the different Ca^{2+}-SCISEs in 10^{-7} M to 10^{-2} M $CaCl_2$ solutions (calibration from low to high concentrations). All electrodes

showed almost Nernstian slopes, which were calculated from the linear part of the calibration curves, and rather similar detection limits (LOD) of (3.4-8.2)×10^{-6} M (Table 2). We determined the reproducibility of the standard potential (E^0) by extrapolating the linear section of the calibration curve to a_{Ca} = 1 (*i.e.* log a_{Ca} = 0). Table 2 summarizes the reproducibility of the different Ca^{2+}-SCISEs. The best reproducibility was obtained for the Ca^{2+}-SCISEs with Meth-PEDOT and Meth-PEDOT (0.2 wt% cMWCNT) as solid-contact showing the lowest standard deviation of E^0 (±13 mV; n = 6). In contrary to other studies [43, 45], our results indicate that we did not obtain any significantly improvements in the potentiometric response of the Ca^{2+}-SCISEs by adding MWCNTs/cMWCNTs to the methacrylate functionalized PEDOT-SC. This discrepancy can be related to the fact that the transduction mechanism (*i.e.* oxidation and reduction reaction) of the SC is limited by the PU-ISM. This is probably due to the much higher bulk resistance of the PU-ISM (86-117 MΩ) compared to the plasticized PVC-ISM (usually ca. 2-5 MΩ) [19, 40], indicating that the diffusion coefficients of ionic species are lower in the PU-ISM. It cannot therefore provide the SC with a sufficient amount of charge compensating anions or/and cations .Fig. S3 shows the potential traces of the Ca^{2+}-SCISE with Meth-PEDOT in order to illustrate the short-time potential stability and the response time of the sensor.

The selectivity coefficients of the Ca^{2+}-SCISEs towards Na^+, K^+, Mg^{2+} and Li^+ were determined by the mixed solution method in the presence of 0.1 M background concentration of the interfering ions (Table S2). We obtained the following selectivity coefficients log K_{Ca^{2+},Na^+} = -3.3, log K_{Ca^{2+},K^+} = -3.4, log K_{Ca^{2+},Li^+} = -3.1 and log $K_{Ca^{2+},Mg^{2+}}$ = -3.8. These values are in good agreement with previously reported selectivity coefficients for ISFETs and Ca^{2+}-SCISEs with the same ISM composition as used in this work [32, 38]. This indicates that the selectivity of the Ca^{2+}-SCISEs is not influenced by the type of the SC. It may be mentioned that ISE with PVC membranes prepared with 2-nitrophenyl octyl plasticizer show better selectivity [46]. However, it is not possible to use compounds containing nitro-group in formulations of photocurable polymers as this nitro-group inhibits the radical initiation of the polymerization.

3.5. Potentiometric aqueous layer test.

One of the major problems of SCISEs is penetration of water through the polymer membrane and its condensation at the membrane/SC interface. This produces instabilities in sensor response and membrane adhesion failure. The water layer/pool formation at the interface PU-ISM/SC was studied by the potentiometric aqueous layer test, in which the potential drifts of the Ca^{2+}-SCISEs were measured in primary and interfering ion solutions for more than 20 h [47]. As can be seen in Fig. 5b, Ca^{2+}-SCISEs prepared with and without MWCNT showed rather stable potentials and relatively quick recovery of the sensor signal after changing the solutions. This indicates that the cross-linking between the SCs and the ISM prevents the aqueous layer formation at the PU-ISM/SC interface.

3.6. Oxygen, carbon dioxide and light sensitivity of the Ca^{2+}-SCISEs.

We also investigated the influence of oxygen (O_2) and carbon dioxide (CO_2) on the potential stability of the Ca^{2+}-SCISEs which are of fundamental importance to optimize the performance of the sensors. Fig. S4 reveals that all the Ca^{2+}-SCISEs showed practically no O_2 sensitivity and negligible CO_2 sensitivity. In order to determine the light sensitivity, the potential drift of the Ca^{2+}-SCISEs were measured when the illumination conditions changed from darkness, room light to cold light. Fig. S5 shows stable electrode potentials for the Ca^{2+}-SCISEs prepared with Meth-PEDOT and Meth-PEDOT containing 0.2wt % cMWCNT, whereas the electrodes prepared with Meth-PEDOT-MWCNT showed a minor potential drift during the first hour after the illumination was changed from dark to room light. We conclude that the Ca^{2+}-SCISEs based on Meth-PEDOT and Meth-PEDOT containing cMWCNT are not light sensitive under normal measurement conditions in room light.

3.7. Durability of the Ca^{2+}-SCISEs

To check the quality of the membrane/conducting polymer interface formed by copolymerization in prevention of water penetration Ca^{2+}-SCISEs were kept in constant contact with 10^{-3} M $CaCl_2$ solution during three months. After this period of time it was found that all electrodes except those prepared with Meth-PEDOT containing 0.2 wt% MWCNT (no response) and 0.5 wt% cMWCNT show close to Nernstian slopes of 26±1 mV/pCa^{2+}. The Meth-PEDOT-0.2 % MWCNT lost it response and sensors with 0.5 % cMWCNT showed sensitivity less than 20

mV/decade. The average E^0 drift during this time was ca. 2 mV per day and detection limits remained as low as 5 $\times 10^{-6}$ M. These data confirm that the cross-linking between the conductive Meth-PEDOT-SC and the PU-ISM gives SCISEs with a relatively long lifetime compared with other developed SCISES which have lifetime between 2 and 6 month [48-50]. These results also show that the adhesion between the ISM and the screen-printed substrate is excellent.

4. Conclusions

We report here a low-cost and simple fabrication method of disposable Ca-ion sensors based on ISE with solid contact formed by Meth-PEDOT and Meth-PEDOT-MWCNT/cMWCNT conducting polymer films. Electrochemical characterization was performed using cyclic voltammetry, electrochemical impedance measurements and potentiometric measurements. The results of CV and EIS experiments reveal that the Meth-PEDOT-cMWCNT has a higher redox capacitance than Meth-PEDOT-MWCNT and Meth-PEDOT. However, after coating the solid contacts with a photo-cured polyurethane-based Ca^{2+}-selective membrane (ISM) the redox capacitance of the solid contact was essentially limited by the high bulk resistance of the ISM. Consequently, no significant improvements in potentiometric response of the Ca^{2+}-SCISEs were obtained by adding MWCNT into the conducting polymer films in terms of sensitivity, selectivity, LOD, lifetime as well as robustness to the influence of light, O_2 and CO_2. No aqueous layer formation was detected at the interfaces between the solid-contacts and the membranes of the Ca^{2+}-SCISEs by using the water layer test. Based on the results of this work it can be concluded that Meth-PEDOT is a promising solid-contact material to develop low-cost and easy to prepare ISEs.

Acknowledgments

This work was supported by the People Programme (Marie Curie Actions) of the 7th Framework Programme of the European Union (FP7/2007-2013) under REA grant agreement no. 600388 (TECNIOspring programme) and from the Agency for Business Competitiveness of the Government of Catalonia (ACCIÓ). N.A. also acknowledges the Government of Russian Federation (Grant 074-U01)

References

[1] Stenger-Smith JD. Intrinsically electrically conducting polymers. Synthesis, characterization, and their applications. Progress in Polymer Science 1998;23:57-79.
[2] Patil AO, Heeger AJ, Wudl F. Optical-properties of conducting polymers Chemical reviews 1988;88:183-200.
[3] Jelle BP, Hagen G. Electrochemical multilayer deposition of polyaniline and Prussian Blue and their application in solid state electrochromic windows. Journal of Applied Electrochemistry 1998;28:1061-5.
[4] Pei Q, Zuccarello G, Ahlskog M, Inganäs O. Electrochromic and highly stable poly(3,4-ethylenedioxythiophene) switches between opaque blue-black and transparent sky blue. Polymer 1994;35:1347-51.
[5] Reddinger JL, Sotzing GA, Reynolds JR. Muticoloured electrochromic polymers derived from easily oxidized bis[2-(3,4-ethylenedioxy)thienyl]carbazoles. Chemical Communications 1996:1777-8.
[6] Qiu Y, Duan L, Wang LD. Flexible organic light-emitting diodes with poly-3,4-ethylenedioxythiophene as transparent anode. Chin Sci Bull 2002;47:1979-82.
[7] Yu LS, Chen SA. High efficiency polymer light emitting diodes based on poly(phenylene vinylene)s with balanced electron and hole fluxes. Synth Met 2002;132:81-6.
[8] Paik KL, Baek NS, Kim HK, Lee JH, Lee Y. White light-emitting diodes from novel silicon-based copolymers containing both electron-transport oxadiazole and hole-transport carbazole moieties in the main chain. Macromolecules 2002;35:6782-91.
[9] Meyer WH. Polymer electrolytes for lithium-ion batteries. Advanced Materials 1998;10:439.
[10] Gurunathan K, Murugan AV, Marimuthu R, Mulik UP, Amalnerkar DP. Electrochemically synthesised conducting polymeric materials for applications towards technology in electronics, optoelectronics and energy storage devices. Mater Chem Phys 1999;61:173-91.
[11] Conway BE. Transition from supercapacitor to battery behavior in electrochemical energy-storage J Electrochem Soc 1991;138:1539-48.
[12] Kros A, Nolte RJM, Sommerdijk N. Conducting polymers with confined dimensions: Track-etch membranes for amperometric biosensor applications. Advanced Materials 2002;14:1779-82.
[13] Dall'Antonia LH, Vidotti ME, de Torresi SIC, Torresi RM. A new sensor for ammonia determination based on polypyrrole films doped with dodecylbenzenesulfonate (DBSA) ions. Electroanalysis 2002;14:1577-86.
[14] Chaubey A, Gerard M, Singhal R, Singh VS, Malhotra BD. Immobilization of lactate dehydrogenase on electrochemically prepared polypyrrole-polyvinylsulphonate composite films for application to lactate biosensors. Electrochimica Acta 2000;46:723-9.
[15] Lindfors T, Ervela S, Ivaska A. Polyaniline as pH-sensitive component in plasticized PVC membranes. Journal of Electroanalytical Chemistry 2003;560:69-78.
[16] Gyurcsanyi RE, Nyback AS, Toth K, Nagy G, Ivaska A. Novel polypyrrole based all-solid-state potassium-selective microelectrodes. Analyst 1998;123:1339-44.

[17] Michalska A, Hulanicki A, Lewenstam A. All-solid-state potentiometric sensors for potassium and sodium based on poly(pyrrole) solid contact. Microchemical Journal 1997;57:59-64.
[18] Cadogan A, Gao Z, Lewenstam A, Ivaska A, Diamond D. All-solid-state sodium-selective electrode based on a calixarene ionophore in a poly(vinyl chloride) membrane with a polypyrrole solid contact. Analytical Chemistry 1992;64:2496-501.
[19] Peramo A, Urbanchek MG, Spanninga SA, Povlich LK, Cederna P, Martin DC. In situ polymerization of a conductive polymer in acellular muscle tissue constructs. Tissue Eng Part A 2008;14:423-32.
[20] Richardson-Burns SM, Hendricks JL, Martin DC. Electrochemical polymerization of conducting polymers in living neural tissue. J Neural Eng 2007;4:L6-L13.
[21] Elschner A, Kirchmeyer S, Lövenich W, Merker U, Reuter K. PEDOT. Principles and Applications of an Intrinsically Conductive Polymer 2011.
[22] Alshammari AS, Shkunov M, Silva SRP. Correlation between wetting properties and electrical performance of solution processed PEDOT:PSS/CNT nano-composite thin films. Colloid and Polymer Science 2014;292:661-8.
[23] Lindfors T, Latonen R-M. Improved charging/discharging behavior of electropolymerized nanostructured composite films of polyaniline and electrochemically reduced graphene oxide. Carbon 2014;69:122-31.
[24] Sundfors F, Bereczki R, Bobacka J, Toth K, Ivaska A, Gyurcsanyi RE. Microcavity based solid-contact ion-selective microelectrodes. Electroanalysis 2006;18:1372-8.
[25] Gyurcsanyi RE, Rangisetty N, Clifton S, Pendley BD, Lindner E. Microfabricated ISEs: critical comparison of inherently conducting polymer and hydrogel based inner contacts. Talanta 2004;63:89-99.
[26] Zhang JX, Guo YX, Li SJ, Xu H. A solid-contact pH-selective electrode based on tridodecylamine as hydrogen neutral ionophore. Meas Sci Technol 2016;27:9.
[27] Sjoberg P, Määttänen A, Vanamo U, Novell M, Ihalainen P, Andrade FJ, et al. Paper-based potentiometric ion sensors constructed on ink-jet printed gold electrodes. Sens Actuator B-Chem 2016;224:325-32.
[28] Apostu M, Bibire N, Tantaru G, Vieriu M, Panainte AD, Agoroaei L. Ion-selective Membrane Electrodes for the Determination of Heavy Metals Construction characterization and applications. Rev Chim 2015;66:657-9.
[29] He N, Lindfors T. Determination of Water Uptake of Polymeric Ion-Selective Membranes with the Coulometric Karl Fischer and FT-IR-Attenuated Total Reflection Techniques. Analytical Chemistry 2013;85:1006-12.
[30] Abramova N, Bratov A. Application of Photocured Polymer Ion Selective Membranes for Solid-State Chemical Sensors. Chemosensors 2015;3:190-9.
[31] Beltran A, Artigas J, Jimenez C, Mas R, Bartroli J, Alonso J. Development of durable nitrate-selective membranes for all-solid state ISE and ISFET sensors based on photocurable compositions. Electroanalysis 2002;14:213-20.
[32] Abramova N, Moral-Vico J, Soley J, Ocana C, Bratov A. Solid contact ion sensor with conducting polymer layer copolymerized with the ion-selective membrane for determination of calcium in blood serum. Analytica Chimica Acta 2016;943:50-7.
[33] Reinhoudt DN, Engbersen JFJ, Brzozka Z, van der Vlekkert HH, Honig GWN, Holterman HAJ, et al. Development of Durable K+-Selective Chemically Modified

Field Effect Transistors with Functionalized Polysiloxane Membranes. Analytical Chemistry 1994;66:3618-23.
[34] Abramova N, Bratov A. Photocurable pH-sensitive membrane for ion-selective field effect transistors. Talanta 2010;81:208-12.
[35] Cha GS, Liu D, Meyerhoff ME, Cantor HC, Midgley AR, Goldberg HD, et al. Electrochemical Performance, Biocompatibility, and adhesion of new polymer matrices for solid-state ion sensors. Analytical Chemistry 1991;63:1666-72.
[36] Rzewuska A, Wojciechowski M, Bulska E, Hall EAH, Maksymiuk K, Michalska A. Composite Polyacrylate–Poly(3,4- ethylenedioxythiophene) Membranes for Improved All-Solid-State Ion-Selective Sensors. Anal Chem 2008;80:321-7.
[37] Bratov A, Abramova N, Mu¤oz J, Dominguez C, Alegret S, Bartroli J. Photocurable polymer matrices for potassium-sensitive ion- selective electrode membranes. AnalChem 1995;67:3589-95.
[38] Abramova N, Bratov A, Ipatov A, Levichev S, Aris A, Rodriguez EM. New flow-through analytical system based on ion-selective field effect transistors with optimised calcium selective photocurable membrane for bovine serum analysis. Talanta 2013;113:31-5.
[39] Bobacka J. Potential stability of all-solid-state ion-selective electrodes using conducting polymers as ion-to-electron transducers. Analytical Chemistry 1999;71:4932-7.
[40] Guilbault G, Durst RA, Frant MS, Freiser H, Hansen EH, Light TS, et al. Pure Appl Chem 1976;46:127-32.
[41] Bobacka J. Conducting polymer-based solid-state ion-selective electrodes. Electroanalysis 2006;18:7-18.
[42] Bobacka J, Lewenstam A, Ivaska A. Electrochemical impedance spectroscopy of oxidized poly(3,4-ethylenedioxythiophene) film electrodes in aqueous solutions. Journal of Electroanalytical Chemistry 2000;489:17-27.
[43] Mousavi Z, Bobacka J, Lewenstam A, Ivaska A. Poly(3,4-ethylenedioxythiophene) (PEDOT) doped with carbon nanotubes as ion-to-electron transducer in polymer membrane-based potassium ion-selective electrodes. Journal of Electroanalytical Chemistry 2009;633:246-52.
[44] McDonald JR. Impedance Spectroscopy. New York: John Wiley; 1987.
[45] Mousavi Z, Teter A, Lewenstam A, Maj-Zurawska M, Ivaska A, Bobacka J. Comparison of Multi-walled Carbon Nanotubes and Poly(3-octylthiophene) as Ion-to-Electron Transducers in All-Solid-State Potassium Ion-Selective Electrodes. Electroanalysis 2011;23:1352-8.
[46] Schefer U, Ammann D, Pretsch E, Oesch U, Simon W. Neutral carrier based calcium(2+)-selective electrode with detection limit in the sub-nanomolar range. Anal Chem 1986;58:2282-5.
[47] Fibbioli M, Morf WE, Badertscher M, de Rooij NF, Pretsch E. Potential drifts of solid-contacted ion-selective electrodes due to zero-current ion fluxes through the sensor membrane. Electroanalysis 2000;12:1286-92.
[48] Wagner M, Lisak G, Ivaska A, Bobacka J. Durable PEDOT:PSS films obtained from modified water-based inks for electrochemical sensors. Sensors and Actuators B: Chemical 2013;181:694-701.
[49] Xu H, Wang Y, Luo ZY, Pan YW. A miniature all-solid-state calcium electrode applied to in situ seawater measurement. Meas Sci Technol 2013;24:6.

[50] Matusevich A, Pietrzak M, Malinowska E. Miniaturized F--selective all-solid-state potentiometric sensors with conductive polymer as an intermediate layer. Sens Actuator B-Chem 2012;168:62-73.

Table

Table 1. Results of the chronopotentiometry measurements with the Ca^{2+}-SCISEs where R, $\Delta E/\Delta t$ and C_L are the bulk resistance of the ISM, potential drift of the Ca^{2+}-SCISEs and the redox capacitance of the SC. We also show for comparison the redox capacitances of the bare Meth-PEDOT and Meth-PEDOT-MWCNT/cMWCNT solid-contacts (prepared on screen-printed electrodes, without ISM) obtained for from CV (C_{CV}) and EIS (C_{EIS}) measurements.

wt% MWCNT	wt% cMWCNT	R (MΩ)	$\Delta E/\Delta t$ (µV/s)	C_L (µF)	C_{CV} (µF)	C_{EIS} (µF)
-	-	89.1	34.4	29.1 ± 8.2	400	- [a]
0.2	-	89.3	21.1	47.3 ± 7.9	521	250
0.5	-	91.1	21.9	45.7 ± 11	943	382
-	0.2	116.8	28.2	35.3 ± 9.2	980	610
-	0.5	85.7	33.3	30.0 ± 10	3070	2475

[a] Value not available, because EIS data were not fitted to the equivalent circuit.

Table 2. Reproducibility of the standard potential (E^0), potentiometric slopes (S) of the linear part of the calibration curves and the detection limit (LOD) for the Ca^{2+}-SCISEs (n = 6).

wt % MWCNT	wt % cMWCNT	E^0 (mV)	S (mV/pCa)	LOD (M)
-	-	429.2 ± 12.9	28.8 ± 0.8	$(8.2 \pm 2.1)\cdot 10^{-6}$
0.2	-	422.4 ± 50.2	29.3 ± 1.0	$(3.4 \pm 3.1)\cdot 10^{-6}$
0.5	-	461.4 ± 16.3	30.3 ± 1.9	$(7.8 \pm 3.9)\cdot 10^{-6}$
-	0.2	484.9 ± 13.2	30.6 ± 0.7	$(6.3 \pm 2.0)\cdot 10^{-6}$
-	0.5	366.6 ± 37.0	29.3 ± 1.9	$(7.1 \pm 2.4)\cdot 10^{-6}$

Figure Captions

Figure 1. CVs of screen-printed Meth-PEDOT electrodes containing: (1) 0 wt% MWCNT/cMWCNT, (2) 0.2 wt% MWCNT, (3) 0.5 wt% MWCNT, (4) 0.2 wt% cMWCNT and (5) 0.5 wt% cMWCNT; CVs show the 100^{th} cycle in 0.1 M KNO_3 with $\nu = 10$ mV s^{-1}.

Figure 2. a) Electrochemical impedance spectra of the screen-printed Meth-PEDOT electrodes containing: (1) 0 wt% MWCNT/cMWCNT, (2) 0.2 wt% MWCNT, (3) 0.5 wt% MWCNT, (4) 0.2 wt% cMWCNT and (5) 0.5 wt% cMWCNT. The spectra were measured at the open circuit potential (E_{dc}) in 0.1 M KNO_3 with $\Delta E_{ac} = 10$ mV and f = 100 kHz – 10 mHz. **b)** The equivalent circuit used for fitting the impedance spectra where R, Z_D and CPE are the solution resistance, finite-length Warburg diffusion element and constant phase element, respectively.

Figure 3. Potentiometric response of screen-printed Meth-PEDOT solid-contacts containing either MWCNTs or cMWCNTs in 10^{-8}-10^{-1} M KNO_3: (1) 0 wt% MWCNT/cMWCNT, (2) 0.2 wt% MWCNT, (3) 0.5 wt% MWCNT, (4) 0.2 wt% cMWCNT and (5) 0.5 wt% cMWCNT.

Figure 4. Chronopotentiograms of the Ca^{2+}-SCISEs prepared with the Meth-PEDOT solid-contacts containing: (1) 0 wt% MWCNT/cMWCNT, (2) 0.2 wt% MWCNT, (3) 0.5 wt% MWCNT, (4) 0.2 wt% cMWCNT and (5) 0.5 wt% cMWCNT. The measurements were done in 0.1 M $CaCl_2$ by first applying +1 nA for 60 s and then -1 nA for 60 s.

Figure 5. **a)** Calibrations plots of the Ca^{2+}-SCISEs in 10^{-7} to 10^{-2} M $CaCl_2$ solution. **b)** The potentiometric aqueous layer test in 0.1 M primary ion (Ca^{2+}) and interfering ion (Na^{+}) solutions for the Ca^{2+}-SCISEs prepared with the Meth-PEDOT solid-contacts containing: (1) 0 wt% MWCNT/cMWCNT, (2) 0.2 wt% MWCNT, (3) 0.5 wt% MWCNT, (4) 0.2 wt% cMWCNT and (5) 0.5 wt% cMWCNT. Dotted line represents the ideal Nernstian plot.

Figure
Click here to download high resolution image

Figure 1

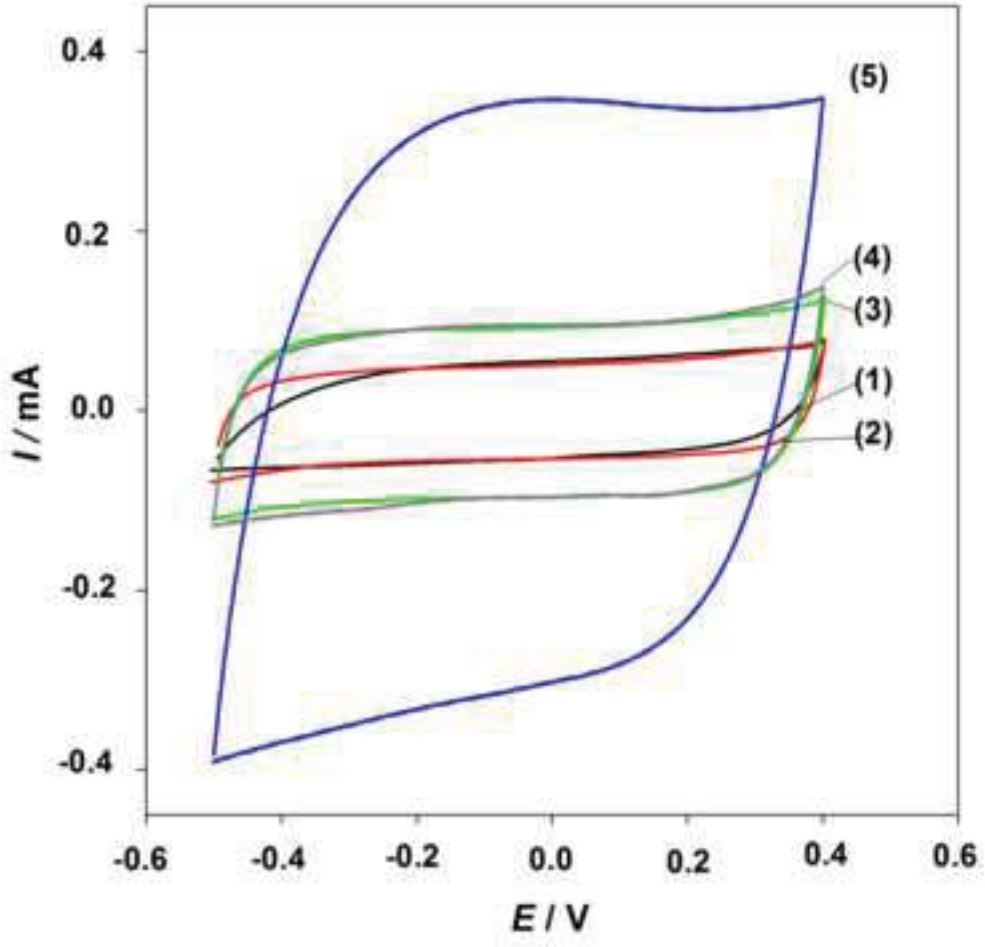

Figure
Click here to download high resolution image

Figure 2

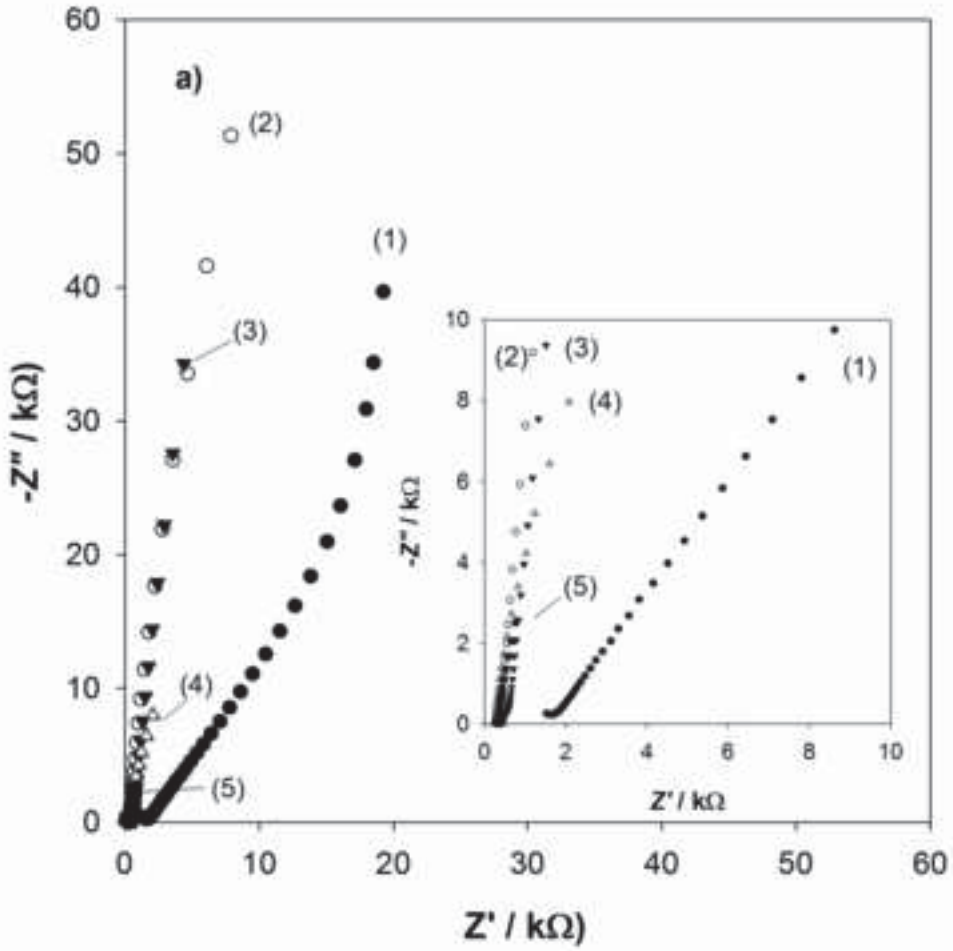

b)

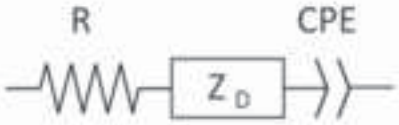

Figure
Click here to download high resolution image

Figure 3

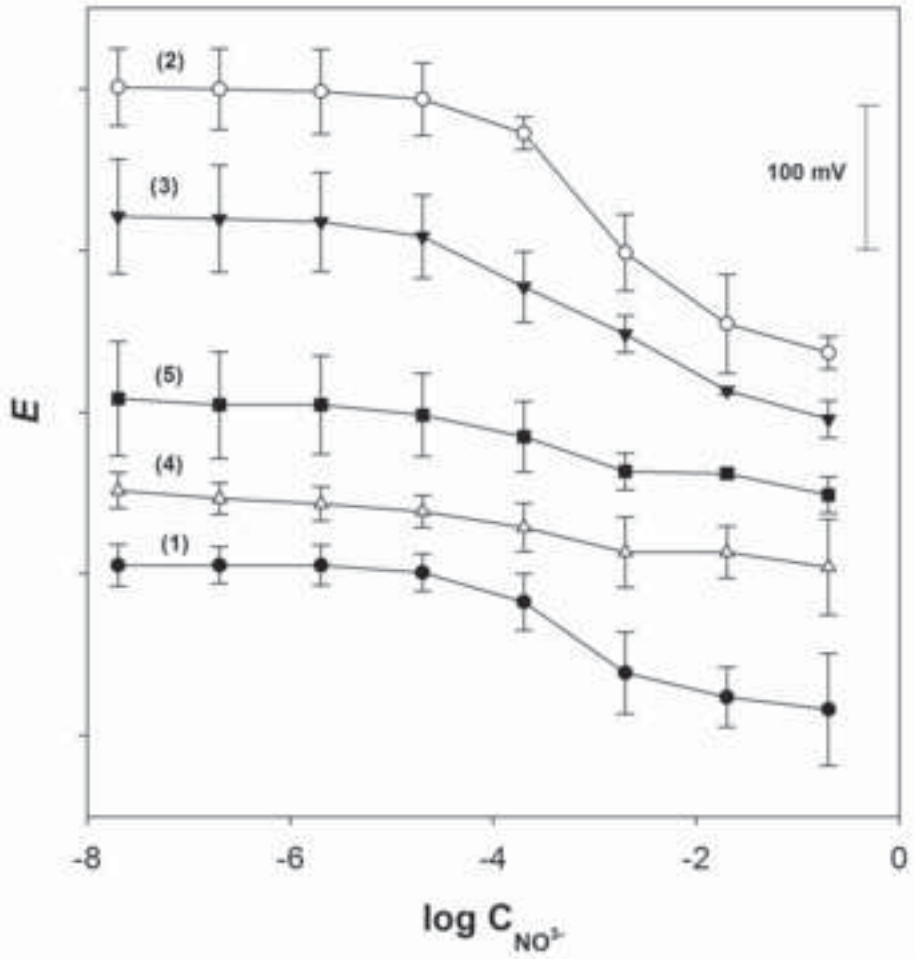

Figure
Click here to download high resolution image

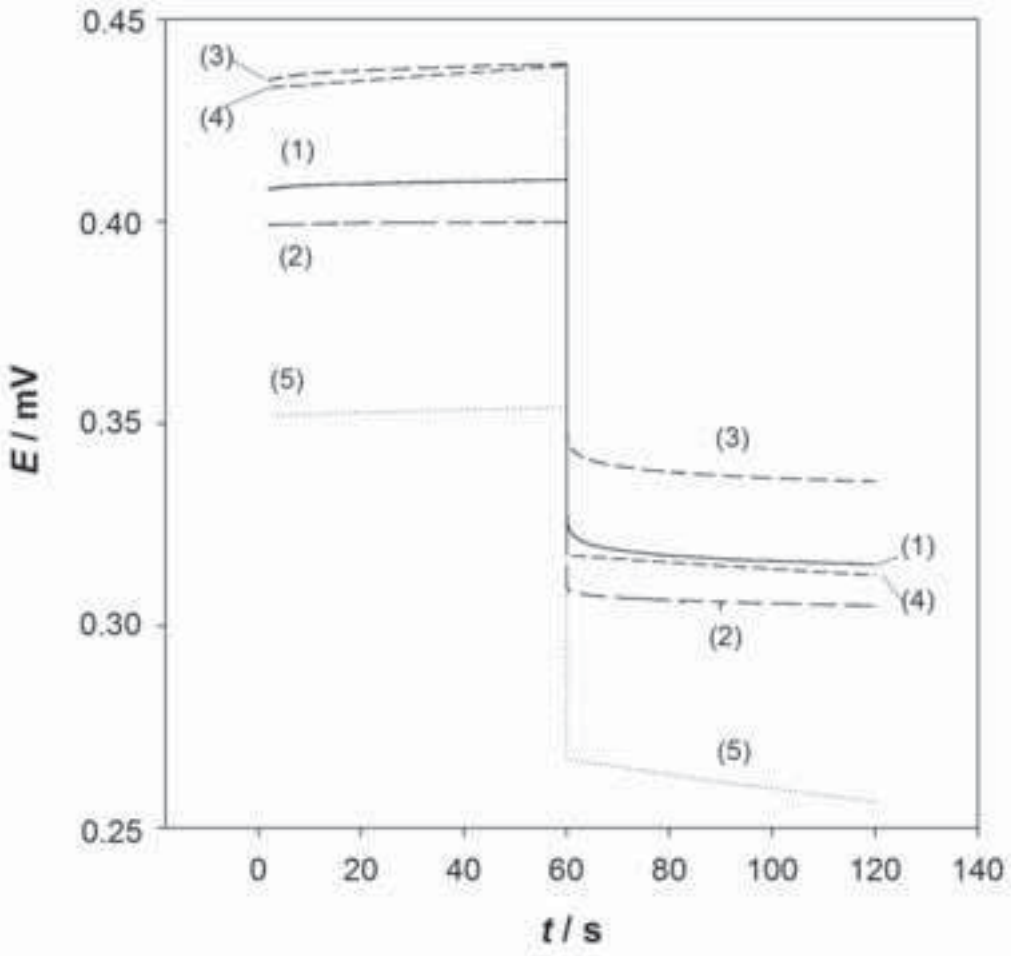

Figure
Click here to download high resolution image

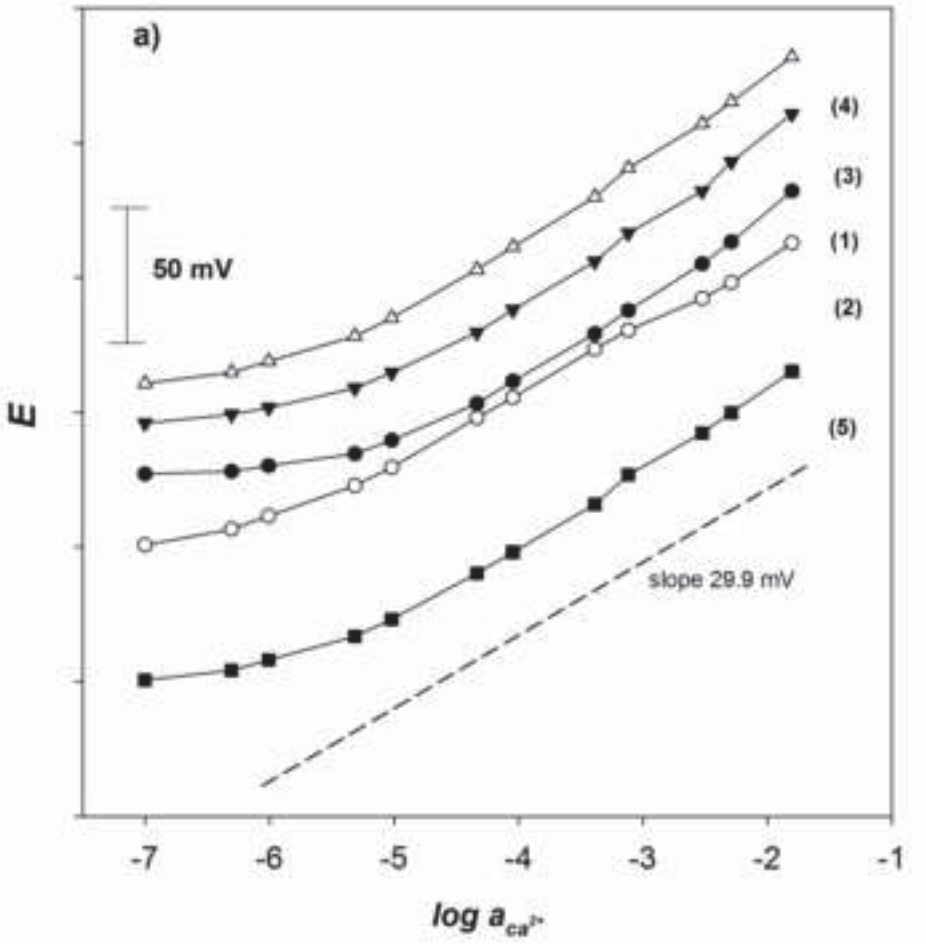

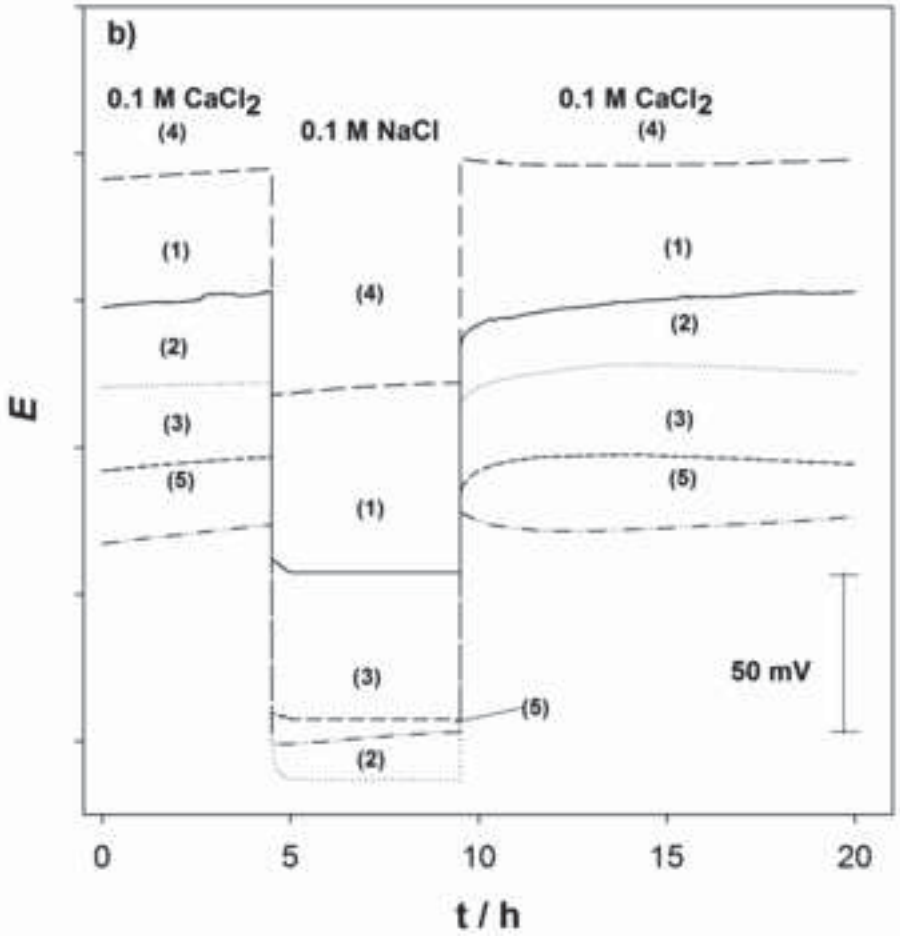

Supplementary Material

Click here to download Supplementary Material: 20171126_Supporting Information_Revised.docx

*Graphical Abstract (for review)

Click here to download high resolution image